REPORT DOCUMENTATION PAGE

Form Approved
OMB No. 0704-0188

PLEASE DO NOT RETURN YOUR FORM TO THE ABOVE ORGANIZATION.

1. REPORT DATE *(DD-MM-YYYY)*	2. REPORT TYPE	3. DATES COVERED *(From - To)*
04-03-2014	Journal Article	

4. TITLE AND SUBTITLE
Observed Volume Fluxes and Mixing in the Dardanelles Strait

5a. CONTRACT NUMBER

5b. GRANT NUMBER

5c. PROGRAM ELEMENT NUMBER
0601153N

6. AUTHOR(S)
Ewa Jarosz, William J. Teague, Jeffrey W. Book and Sukru T. Besiktepe

5d. PROJECT NUMBER

5e. TASK NUMBER

5f. WORK UNIT NUMBER
73-4491-03-5

7. PERFORMING ORGANIZATION NAME(S) AND ADDRESS(ES)
Naval Research Laboratory
Oceanography Division
Stennis Space Center, MS 39529-5004

8. PERFORMING ORGANIZATION REPORT NUMBER
NRL/JA/7330--13-1691

9. SPONSORING/MONITORING AGENCY NAME(S) AND ADDRESS(ES)
Office of Naval Research
One Liberty Center
875 North Randolph Street, Suite 1425
Arlington, VA 22203-1995

10. SPONSOR/MONITOR'S ACRONYM(S)
ONR

11. SPONSOR/MONITOR'S REPORT NUMBER(S)

12. DISTRIBUTION/AVAILABILITY STATEMENT
Approved for public release, distribution is unlimited.

20151013129

13. SUPPLEMENTARY NOTES

14. ABSTRACT
Pairs of moorings equipped with current profilers were deployed at each end of the Dardanelles Strait and remained in place for over 13 months. Current observations were able to resolve well the exchange flow and volume fluxes. Volume fluxes showed distinct temporal variability in upper and lower layers, especially evident on synoptic time scales. The synoptic flux variability in the upper layer was coherent with the local atmospheric forcing and the bottom pressure anomaly gradient, while the flux variations in the lower layer were related to the bottom pressure anomaly gradient. Estimated volume flux values were often two or more times larger than their respective annual means. Annual upper-layer flux means were 25.66 × 10^{-3} and 36.68 × 10^{-3} Sv, whereas the lower-layer averages were 14.02 × 10^{-3} and 31.67 × 10^{-3} Sv for the Marmara and Aegean sections, respectively. The fluxes also showed that there was a net low-salinity water outflow to the Aegean Sea, and that they varied weakly on longer time scales (monthly to seasonal). High-salinity water fluxes (≥ 39 psu) were used to calculate strait-averaged vertical eddy diffusivities which ranged between 10^{-4} and 10^{-2} m^2 s^{-1}. Additionally, microstructure observations were used to evaluate vertical eddy diffusivities. These estimates indicated that mixing in the strait varied spatially and temporarily, and it was dependent on complex strait geometry, exchange flow status, and partially on meteorological conditions.

15. SUBJECT TERMS
dardanelles strait, volume fluxes, mixing

16. SECURITY CLASSIFICATION OF:			17. LIMITATION OF ABSTRACT	18. NUMBER OF PAGES	19a. NAME OF RESPONSIBLE PERSON
a. REPORT	b. ABSTRACT	c. THIS PAGE			Ewa Jarosz
Unclassified	Unclassified	Unclassified	UU	15	19b. TELEPHONE NUMBER *(Include area code)* (228) 688-4292

JOURNAL OF GEOPHYSICAL RESEARCH: OCEANS, VOL. 118, 5007–5021, doi:10.1002/jgrc.20396, 2013

Observed volume fluxes and mixing in the Dardanelles Strait

Ewa Jarosz,[1] William J. Teague,[1] Jeffrey W. Book,[1] and Şükrü T. Beşiktepe[2]

Received 19 June 2013; revised 4 September 2013; accepted 5 September 2013; published 4 October 2013.

[1] Pairs of moorings equipped with current profilers were deployed at each end of the Dardanelles Strait and remained in place for over 13 months. Current observations were able to resolve well the exchange flow and volume fluxes. Volume fluxes showed distinct temporal variability in upper and lower layers, especially evident on synoptic time scales. The synoptic flux variability in the upper layer was coherent with the local atmospheric forcing and the bottom pressure anomaly gradient, while the flux variations in the lower layer were related to the bottom pressure anomaly gradient. Estimated volume flux values were often two or more times larger than their respective annual means. Annual upper-layer flux means were 25.66×10^{-3} and 36.68×10^{-3} Sv, whereas the lower-layer averages were 14.02×10^{-3} and 31.67×10^{-3} Sv for the Marmara and Aegean sections, respectively. The fluxes also showed that there was a net low-salinity water outflow to the Aegean Sea, and that they varied weakly on longer time scales (monthly to seasonal). High-salinity water fluxes ($\geq$ 39 psu) were used to calculate strait-averaged vertical eddy diffusivities which ranged between 10^{-4} and 10^{-2} m^2 s^{-1}. Additionally, microstructure observations were used to evaluate vertical eddy diffusivities. These estimates indicated that mixing in the strait varied spatially and temporarily, and it was dependent on complex strait geometry, exchange flow status, and partially on meteorological conditions. Large values of eddy diffusivities, with a depth-averaged mean of 1.3×10^{-2} m^2 s^{-1}, and vigorous mixing were found in the Nara Pass, the narrowest section in the Dardanelles Strait.

Citation: Jarosz, E., W. J. Teague, J. W. Book, and Ş. T. Beşiktepe (2013), Observed volume fluxes and mixing in the Dardanelles Strait, *J. Geophys. Res. Oceans*, *118*, 5007–5021, doi:10.1002/jgrc.20396.

1. Introduction

[2] The Dardanelles Strait is a part of the Turkish Strait System (TSS) that connects the Aegean/Mediterranean Sea waters to the Black Sea. The mean flow regime in the strait is a two-layer exchange with brackish waters originating in the Black Sea flowing in the upper layer and salty waters from the Aegean Sea moving approximately northeastward in the lower layer [*Ünlüata et al.*, 1990; *Tuğrul et al.*, 2002; *Jarosz et al.*, 2012]. The sum of riverine discharge and precipitation is not balanced by evaporation in the Black Sea. Consequently, there is a net surplus of low-salinity waters from the Black Sea that reaches the Aegean Sea every year through the TSS. This surplus was estimated to be between 0.006 Sv (1Sv = 10^6 m^3 s^{-1}) and 0.01 Sv [*Ünlüata et al.*, 1990; *Simonov and Altman*, 1991; *Peneva et al.*, 2001; *Kara et al.*, 2008].

[3] It has been recognized for years that the upper-layer outflow from the Dardanelles Strait to the Aegean Sea impacts the surface circulation in the North Aegean Sea [*Poulos et al.*, 1997; *Tzali et al.*, 2010]. *Zervakis et al.* [2000] have indicated that in addition to atmospheric conditions, this outflow also affects the deep water formation in the North Aegean Sea. The outflow produces a layer with a well-defined thickness and distinct hydrographic characteristics (low salinity and low temperature in cold months). As this layer thickens, its impact becomes larger on air-sea fluxes and hence, it can act as a barrier layer preventing underlying denser waters from heat losses during passages of cold atmospheric fronts in winter and subsequently from sinking and contributing to the deep dense water pool in the North Aegean Sea. A role of the outflow as a regulator of the intensity of deep water formation in the region was also postulated by *Gertman et al.* [2006]. Moreover, the lower-layer outflow of high-salinity waters from the Dardanelles Strait to the Sea of Marmara impacts subsurface circulation (below the upper 20–25 m), hydrography, and oxygen distribution in this semienclosed sea [*Beşiktepe et al.*, 1993, 1994; *Beşiktepe*, 2003]. The high-salinity outflow shows distinct seasonal density variability resulting mainly from seasonal temperature changes. In winter, the outflow waters have a higher density than the waters occupying the interior of the sea, and therefore the outflow attaches to the bottom and forms a bottom boundary current entering the interior of the sea as a turbulent plume. In fall, the outflow is lighter than the interior of the sea and manifests itself as a subsurface flow bounded by the upper layer of the Sea of Marmara.

[1]Naval Research Laboratory, Stennis Space Center, Mississippi, USA.
[2]Institute of Marine Sciences and Technology, Dokuz Eylül University, Izmir, Turkey.

Corresponding author: E. Jarosz, Naval Research Laboratory, Stennis Space Center, MS 39529-5004, USA. (ewa.jarosz@nrlssc.navy.mil)

2169-9275/13/10.1002/jgrc.20396

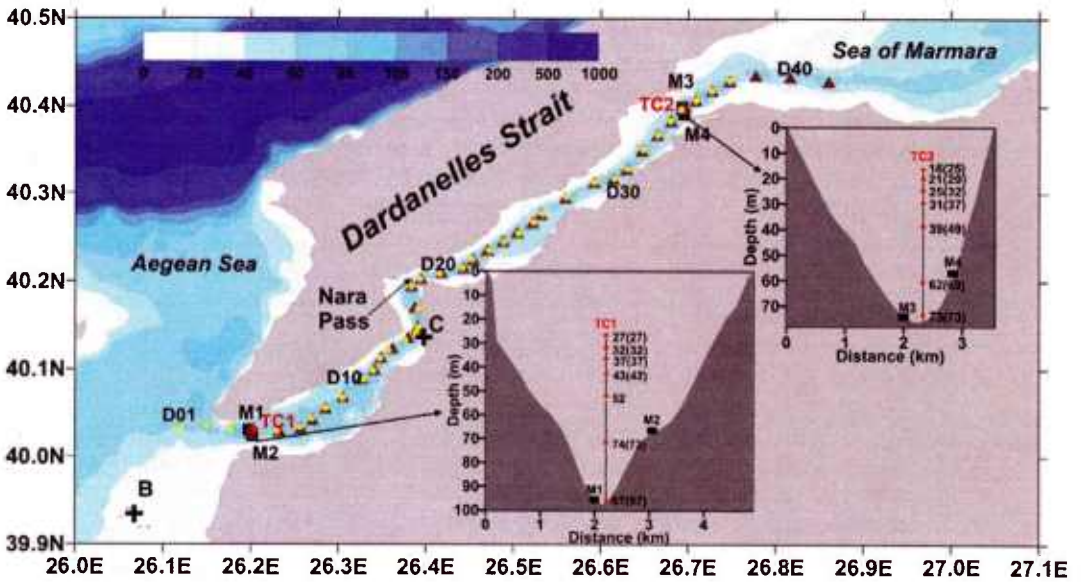

Figure 1. Map of the Dardanelles Strait and the cross sections used in the volume flux estimations (inserts). Moorings, meteorological stations and locations of VMP drops are also shown: Barny moorings (black squares; M1–M4), TC moorings (red diamonds, TC1–TC2; depths (m) of the TC sensors given next to the symbols in the inserts; depths for the second part of the deployment are in parentheses), meteorological stations (black pluses; Çanakkale (C) and Bozcaada (B)), and VMP drop locations (D1–D40; brown triangles—VMP profiles taken on 8 February 2009; yellow dots—VMP profiles taken on 18 February 2009); depth contours are in meters (color bar).

[4] Based on long-term salinity observations along both ends of the Dardanelles Strait, and assuming a steady state mass budget, *Ünlüata et al.* [1990] estimated mean annual volume transports in the upper and lower layers to be 27.46 $\times$ 10^{-3} Sv and 17.95 $\times$ 10^{-3} Sv in the northern Dardanelles (Marmara section) and 39.86 $\times$ 10^{-3} Sv and 30.35 $\times$ 10^{-3} Sv in the southern Dardanelles (Aegean section), respectively. These annual means were later revised, for instance, by *Beşiktepe et al.* [1994] and *Tuğrul et al.* [2002]. *Tuğrul et al.* [2002] also discussed seasonal variability of these volume fluxes. They showed that maximum upper and lower-layer outflows were usually observed in spring, while they were at a minimum in fall.

[5] Until recently, there were no time series of current observations that would allow computation of volume fluxes and evaluation of their variability on a range of time scales. In 2008, the US Naval Research Laboratory (NRL) and the NATO Undersea Research Center (NURC; currently known as the NATO Center for Maritime Research and Experimentation, CMRE) in collaboration with the Turkish Navy Office of Navigation, Hydrography and Oceanography deployed two mooring sections (one at each end) in the Dardanelles Strait as a part of the TSS08 (NURC project) and EPOS (NRL project) programs. The deployment began at the end of August 2008 and ended at the beginning of October 2009 (Figure 1) delivering nearly full water-column current profiles along both ends of the strait for this time period. These continuous observations provide the opportunity to estimate concurrent volume transports at each end of the strait. Time variability of these volume fluxes, possible forcing of the flux fluctuations, and mixing in the strait are discussed in this manuscript. The paper is organized as follows: section 2 describes the analyzed observations. Methodology used to evaluate the volume transport is outlined in section 3. Volume fluxes are presented in section 4. Transport fluctuations and their possible forcing mechanisms are analyzed in section 5. Entrainment and mixing are discussed in sections 6 and 7. Finally, section 8 summarizes the findings.

2. Measurements

[6] Moorings were deployed on 28–29August 2008 and then serviced and redeployed approximately at the same locations in February 2009. Final recovery of all moorings occurred on 11 October 2009. Since locations of the moorings for both deployments were almost identical, observations were combined into a single time series for all presented analyses. Each mooring section (Figure 1) was configured with a bottom-mounted Barny mooring (M1 and M3) and a line mooring (TC1 and TC2) in the deep channel, and another Barny mooring (M2 and M4) in the eastern shallower part of the channel. Barny moorings contained the following instrumentation: an acoustic Doppler current profiler (ADCP), a wave/tide gauge (Sea-Bird Electronics 26), and a conductivity sensor (Sea-Bird Electronics SBE4). All ADCPs were 300 kHz RD Instruments. They recorded current profiles at 1 m vertical resolution. Line moorings (TC1 and TC2) were equipped with Sea-Bird Electronics MicroCats 37 and Aqua Trolls for measuring temperature, conductivity, and pressure (7 instruments on each line). All instruments recorded data at 15 min intervals.

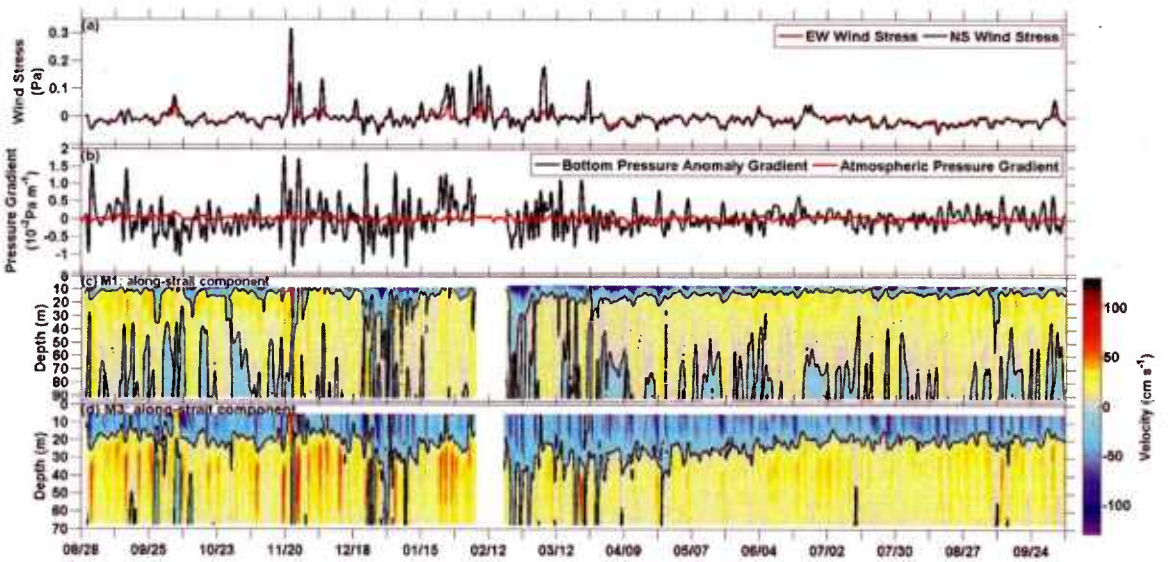

Figure 2. (a) Wind stress components (Pa) estimated from wind observations from Çanakkale (East/West wind stress component: red line, North/South wind stress component: black line), (b) bottom pressure anomaly gradient (black line) and atmospheric pressure gradient (red line) both with units Pa m^{-1}, and along-strait velocity components (cm s^{-1}) from (c) M1 and (d) M3 moorings (positive velocity values are directed toward the Sea of Marmara). High frequencies were removed from the data by applying a 40 h low-pass filter.

[7] Full time series of data were returned from the Barny moorings. Unfortunately, data from the TC1 and TC2 moorings were incomplete because five of the sensors failed and returned limited time series of conductivity or none at all. ADCP observations were interpolated to common depth levels resulting in 1 m vertical resolution. All observations were converted into hourly averages, and high frequency fluctuations (not applicable to the topic of this paper) were eliminated from the data by applying a low-pass filter with a 40 h cutoff frequency. The current observations were also rotated 10° and 50° counterclockwise from east along the southern (Aegean) and northern (Marmara) sections, respectively, to align with along and across-strait coordinate axes. The bottom pressure data allowed an evaluation of pressure variations, p_b' ($p_b' = p_{atm}' + \rho_0 g\eta' + g\int_{-H}^{0} \rho' dz$, where p_{atm}' is the atmospheric pressure, η' is the water level variation, ρ' is the density fluctuation, ρ_0 is the reference density, g is the gravitational acceleration, H is the total depth, and the primes indicate that time means are removed), and an estimation of the bottom pressure anomaly gradient (BPG) (i.e., a bottom pressure variation difference divided by the strait length) between the southern and northern ends of the Dardanelles Strait. Additionally, hourly meteorological observations collected at Turkish land stations, Çanakkale (C), Bozcaada (B), and Tekirdağ (located on the northern shore of the Sea of Marmara, northeast of the area shown in Figure 1), located near the Dardanelles Strait were analyzed. Wind stress estimated from wind observations measured at Çanakkale and atmospheric pressure gradient estimated from observations collected at Bozcaada and Tekirdağ as well as the BPG and along-strait current velocities from M1 and M3 are shown in Figure 2. More detailed descriptions of the EPOS data set and the exchange flow variability in the Dardanelles Strait are in *Jarosz et al.* [2012].

[8] Microstructure observations using a Vertical Microstructure Profiler (VMP) (manufactured by the Rockland Oceanographic Services Inc., Canada and similar to a profiler described by *Wolk et al.* [2002]) were collected during the servicing cruise in February 2009. There were two passes through the deep channel of the strait: on 8 and 18 February 2009 during which a total of 74 microstructure profiles were collected. Figure 1 shows locations of the VMP drops. The VMP profiler carried a thermistor, a microconductivity sensor, two velocity shear probes, a high-resolution pressure sensor, accelerometers, and fine-scale external conductivity (Sea-Bird Electronics SBE4) and temperature (Sea-Bird Electronics SBE3) sensors. VMP profiles extended from a few meters below the surface to the bottom. Moreover, turbulent kinetic energy (TKE) dissipation rates (ε) were estimated from current velocity shear observations following a formula for isotropic turbulence [*Oakey*, 1982]: $\varepsilon = \frac{15}{2}\nu\overline{\left(\frac{\partial u'}{\partial z}\right)^2}$, where ν is the kinematic viscosity, and $\overline{\left(\frac{\partial u'}{\partial z}\right)^2}$ is the variance of the current shear. We recognize that our microstructure data set is inadequate to describe mixing in the Dardanelles Strait in detail. Nevertheless, to the best of our knowledge, these measurements are the only existing turbulence observations taken in this strait; thus, they should provide new insight into mixing there.

3. Methodology for Volume Flux Estimation

[9] The shallowest ADCP bins were approximately 5 m from the surface at both mooring sections. Hence, we employed a vertical current shear approach to extrapolate current velocity from the shallowest bin to the surface. A brief description of the shear approach is as follows: a straight line is fitted to the vertical shear estimated from the upper-layer along-strait currents at each time step, and then the fit is used to evaluate current velocities between the shallowest bin and the surface. We also tried a constant velocity approach that assumes current velocities are constant between the top velocity bin and the surface. As discussed in *Jarosz et al.* [2012], the upper layer is rather thin (on average, 22 m and 13 m in the northern and southern mooring sections, respectively) and the currents tend to respond very swiftly to changing winds. Under conditions of rapidly changing winds, the upper water column tends to be characterized by high vertical current shear, and the shear approach should provide a more realistic approximation of currents near the surface than a constant velocity method. Hence, the shear approach was used to calculate all the volume fluxes. Before integration the velocity data were interpolated and extrapolated onto a grid (1 m in the vertical by 146 m and 200 m in the cross-strait distance for the northern and southern sections, respectively) for every hour, using a triangle-based linear interpolation/extrapolation with the assumption that the velocity at the bottom was zero. Gridded velocity values were then carefully checked to verify that the extrapolation/interpolation procedure produced reasonable values for the region in-between the moorings and near the side walls of the strait.

[10] Salinity observations collected in the northern Dardanelles Strait were used to separate the brackish upper-layer waters from the salty lower-layer waters in this mooring section. First, salinity limits were calculated following an approach given in *Beşiktepe et al.* [1994]: $S_{UL\max} = S_{UL} + 0.2 \cdot (S_{LL} - S_{UL})$ and $S_{LL\min} = S_{UL} + 0.2 \cdot (S_{LL} - S_{UL})$, where S_{UL} and S_{LL} are mean near-surface and near-bottom salinities estimated from observations collected at TC2. The mean of the maximum (S_{ULmax}) and minimum (S_{LLmin}) salinities was 31.6 psu, and this isohaline value was used as the separation between the upper and lower layers in the flux calculations for the Marmara section. This choice was further verified by noting that the depth of the 31.6 psu isohaline followed the 0-velocity depth in this section fairly closely.

[11] In the Aegean section, the TC1 mooring did not extend to shallow enough depths to sample the upper-layer salinity and hence, the approach used in the Marmara section could not be applied there. Instead of using an isohaline, the upper most 0-velocity isotach was used to separate the upper and lower layers for flux calculations in the southern Dardanelles. The first sensor at TC1 was at 27 m and recorded salinities which were generally above 34 psu [*Jarosz et al.*, 2012] indicating that the lower layer waters filled out a major part of the southern section throughout the deployment period. Additionally, historical observations show that salinity of the upper layer is usually below 32 psu near the southern end of the Dardanelles Strait [*Ünlüata et al.*, 1990; *Beşiktepe et al.*, 1994; *Tuğrul et al.*, 2002]. Hence, the upper-layer thickness was reduced to 27 m if the 0-velocity isotach was found to be deeper than 27 m. Overall, the separation of the upper-layer and lower-layer waters is expected to be more accurately estimated for the northern mooring section than for the southern section since the former relies on actual salinity measurements.

[12] Salinity and temperature observations collected over the years in the Dardanelles Strait also clearly indicate that strong mixing occurs in the Nara Pass region. *Ünlüata et al.* [1990] found that over 40% of the high salinity inflow from the Aegean Sea is mixed in and/or entrained into the upper layer and returned back to this sea. To estimate this percentage from the mooring observations during our deployment period we calculated a volume flux budget of waters with salinities of 39 psu or higher. This was done by comparing the volume flux of the high-salinity waters entering the Aegean section to the flux of the high-salinity waters leaving the Marmara section. The bounding depth of the 39-psu waters, which was used in these calculations, was estimated from the salinity time series at both mooring sections (TC1 and TC2).

4. Volume Fluxes

[13] Figure 3 displays time series of the volume fluxes for both layers and the net transport along the northern and southern sections in the Dardanelles Strait. Annual, seasonal, and monthly means of the upper and lower-layer fluxes estimated for the time period between 1 September 2008 and 31 August 2009 are shown in Figure 4. Annual and seasonal means and their root-mean-square (RMS) errors are also listed in Table 1. The RMS errors are defined as the standard deviation divided by the square root of the degrees of freedom. The degrees of freedom are estimated as the sampling period divided by the integral time scale. These errors as given in Table 1 represent the level of statistical uncertainty for assigning perfectly accurate mean fluxes for the time period between 1 September 2008 and 31 August 2009. They do not directly include errors associated with measurement errors and insufficient sampling that led to spatial interpolation and extrapolation of the current velocities in each mooring section. Throughout this manuscript, positive numbers represent a volume flux toward the Sea of Marmara, whereas negative values represent a volume flux toward the Aegean Sea.

[14] On short time scales (synoptic: 2–10 days), temporal variability of all volume fluxes was very evident and pronounced in both layers and along both sections (Figure 3). Fluctuations shown in Figure 3 were often two times or larger than the respective annual means (Figure 4 and Table 1). Additionally, fluxes in both layers completely reversed a number of times. Those events were usually caused by storms passing over the region such as, for instance, one beginning around 3 October 2008 and another moving over the region around 20 November 2008 (Figure 2). The upper-layer flux ranged between -72.98×10^{-3} Sv and 29.46×10^{-3} Sv in the Marmara section and between -82.18×10^{-3} Sv and 47.09×10^{-3} Sv in the Aegean section. The lower-layer flux varied from -26.06×10^{-3} Sv to 73.15×10^{-3} Sv and from -13.69×10^{-3} Sv to 106.93×10^{-3} Sv in the northern and southern Dardanelles Strait, respectively.

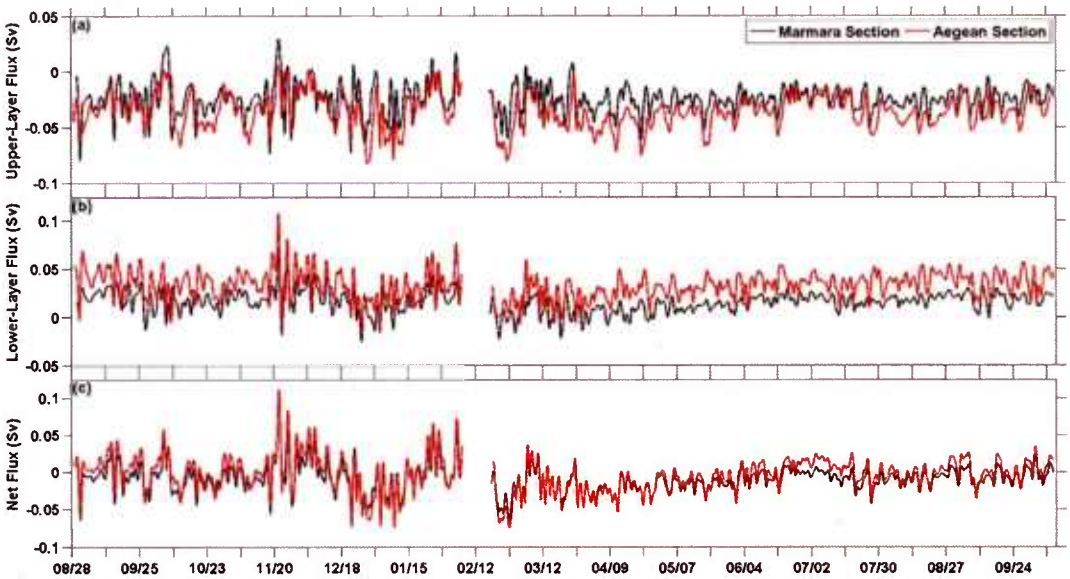

Figure 3. Times series of (a) upper-layer, (b) lower-layer, and (c) net volume fluxes (Sv) in the northern (black lines) and southern (red lines) Dardanelles Strait (positive values—flux toward the Sea of Marmara; negative values—flux toward the Aegean Sea).

[15] Although there was some flux variability on seasonal and monthly time scales (Figure 4 and Table 1), this variability was generally weaker than synoptic variations (Figure 3). Calculated seasonal means also imply that the upper-layer fluxes were at a maximum in spring 2009 and at a minimum in fall 2008, while the opposite was true for the lower-layer fluxes. Additionally, the seasonal cycle was less evident for the upper-layer flux in the Marmara section, but it was very well defined for both layers in the Aegean section and in the lower-layer flux in the Marmara section.

[16] Net fluxes varied significantly throughout the deployment along both mooring sections (Figure 3 and Table 2). In general, fluctuations of the net fluxes at both sections were often similar in amplitudes and directions and changes in their direction were common. Annual means of these fluxes estimated for the time period between

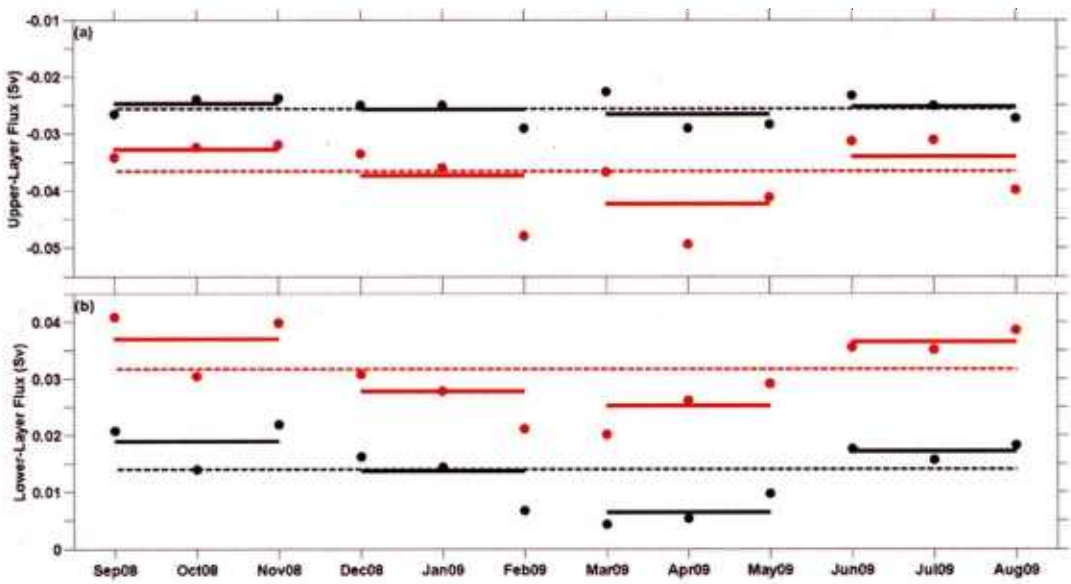

Figure 4. Annual (dashed lines), seasonal (solid thick lines), and monthly (dots) means of volume fluxes (Sv) for the Marmara (black) and Aegean (red) sections estimated from velocity observations recorded between 1 September 2008 and 31 August 2009 (positive values—flux toward the Sea of Marmara; negative values—flux toward the Aegean Sea).

Table 1. Annual and Seasonal Means of Upper and Lower-Layer Volume Fluxes, Their Ranges and Root-Mean-Square (RMS) Errors (All in 10^{-3}Sv) Estimated for the Time Period Between 1 September 2008 and 31 August 2009 (Positive Values—Flux Toward the Sea of Marmara; Negative Values—Flux Toward the Aegean Sea)

Flux Means Flux Range RMS Errors	Northern (Marmara) Section		Southern (Aegean) Section	
	Upper Layer	Lower Layer	Upper Layer	Lower Layer
Annual	−25.66	14.02	−36.68	31.67
	−72.98/29.46	−26.06/73.15	−82.18/4.71	−13.69/106.93
	0.81	1.93	1.74	3.26
Fall 2008	−24.79	18.85	−32.86	36.90
	−72.98/29.46	−19.00/73.15	−67.25/4.71	−12.09/106.93
	1.83	1.18	2.32	1.54
Winter 2008/2009	−25.83	13.64	−37.39	27.67
	−72.37/16.53	−26.06/46.28	−82.18/1.72	−13.69/76.59
	2.00	3.57	3.87	4.23
Spring 2009	−26.73	6.42	−42.42	25.12
	−62.44/7.63	−22.54/25.28	−75.23/−3.34	−8.40/59.32
	1.26	0.95	1.73	1.28
Summer 2009	−25.30	17.16	−34.13	36.40
	−53.11/−8.44	0.83/29.27	−58.33/−13.55	9.20/55.20
	0.84	0.58	1.81	0.99

1 September 2008 and 31 August 2009 were -11.64×10^{-3} Sv (RMS error $= 3.17 \times 10^{-3}$ Sv) and -5.01×10^{-3} Sv (RMS error $= 4.06 \times 10^{-3}$ Sv) for the Marmara and Aegean sections, respectively. These results indicate that there were net outflows toward the Aegean Sea through both sections.

5. Forcing Mechanisms of Volume Flux Fluctuations

[17] Figures 2a and 2b show time series of the wind stress, atmospheric pressure gradient, and the bottom pressure anomaly gradient between southern and northern sections estimated from the bottom pressure measurements after removing record means. All these are considered to be possible driving mechanisms of the flux variations in the Dardanelles Strait. In Figure 2, some correlations between these variables and volume transports are already visually apparent. Strong winds were responsible for blockages and/or reversals of the upper-layer fluxes, while negative values of the BPG were able to significantly reduce and even reverse the lower-layer flux.

[18] To quantify visual comparisons of the concurrent time series of the atmospheric forcing, the BPG, and volume fluxes, and to evaluate relationships among them, spectral analyses were used. Spectra (not shown) of the fluxes indicate that there was enhanced energy at frequencies between 0.1 and 0.6 cycles per day (cpd). Multiple and partial coherences were also computed. Multiple coherence provides the combined coherence between the forcing variables (i.e., the atmospheric forcing and the BPG) and the volume flux, while partial coherences show how coherent the flux variations are with an individual forcing variable after eliminating correlated parts of the signals associated with the other forcing mechanisms from both the forcing variable and the flux. Results from multiple coherence analyses show that wind stresses, bottom pressure anomaly and atmospheric pressure gradients together accounted for, on average, about 71% and 68% of the upper-layer volume flux variance for frequencies less than 0.6 cpd in the Marmara and Aegean sections, respectively (Figure 5). Figure 5 also displays results from partial coherence analyses. These results indicate that the BPG was a primary forcing of flux fluctuations for frequencies higher than 0.25 cpd and 0.3 cpd in the Marmara and Aegean sections, respectively. For lower frequencies, the upper-layer flux variations were driven by a combination of the BPG, atmospheric gradients and along-strait wind stress at the Aegean section, while the along-strait wind stress seemed to mainly drive the fluctuations centered at about 0.1 cpd in the Marmara section.

Table 2. Annual and Seasonal Means of Net Volume Fluxes, Their Ranges and Root-Mean-Square (RMS) Errors (All in 10^{-3}Sv) Estimated for the Time Period From 1 September 2008 to 31 August 2009 (Positive Values—Flux Toward the Sea of Marmara; Negative Values—Flux Toward the Aegean Sea)

Flux Means Flux Range RMS Errors	Northern (Marmara) Section	Southern (Aegean) Section
Annual	−11.64	−5.01
	−73.16/102.24	−75.05/111.35
	3.17	4.06
Fall 2008	−5.94	4.04
	−56.55/102.24	−44.64/111.35
	2.25	2.48
Winter 2008/2009	−12.19	−9.72
	−73.17/53.91	−75.05/72.38
	4.87	7.62
Spring 2009	−20.31	−17.30
	−48.75/20.35	−53.97/36.32
	1.44	2.59
Summer 2009	−8.13	2.27
	−42.85/9.10	−36.02/26.48
	1.11	1.57

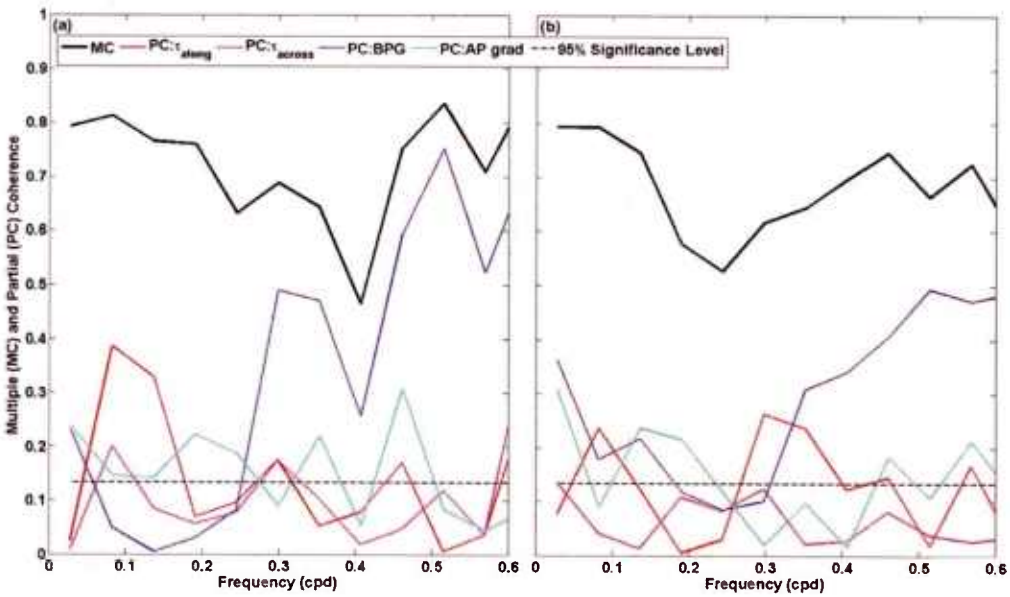

Figure 5. Multiple coherence (MC, black line) and partial coherence (PC, color lines) between the upper-layer volume flux and the bottom pressure anomaly gradient between the southern and northern Dardanelles (blue line), the along (red line) and across-strait (magenta line) wind stress components, and the atmospheric pressure gradient (cyan line) for (a) the Marmara and (b) Aegean sections; the dashed line is the 95% significance level. Wind stresses calculated from winds collected at Çanakkale and the atmospheric pressure gradient estimated from observations from Bozcaada and Tekirdağ were used in the coherence analyses.

[19] Simultaneously, fluctuations observed in the volume fluxes of the lower layer were very coherent with the BPG (Figure 6). In the northern Dardanelles, BPG forcing accounted for on average 64% of the flux variance, whereas it explained about 71% of the flux variability in the southern part of the strait. Note, however, that the ordinary coherence squared between the lower-layer fluxes and the BPG could also include an indirect impact of the atmospheric forcing on these fluxes because this particular statistical approach does not exclude a possible direct influence of the winds and the atmospheric pressure on the observed BPG variability.

6. Entrainment and Mixing From Volume Fluxes

[20] Historical observations of salinity indicate that the upper-layer waters become more saline when traversing the strait. The EPOS salinity and current data allowed calculations of fluxes of high salinity waters (39 psu and higher) as shown in Figure 7a. Year-long averages for the time period between 1 September 2008 and 31 August 2009 were 17.55×10^{-3} Sv (RMS error $= 1.84 \times 10^{-3}$ Sv) and 4.02×10^{-3} Sv (RMS error $= 1.03 \times 10^{-3}$ Sv) in the southern and northern sections, respectively. The difference between these means is 13.53×10^{-3} Sv (RMS error $= 1.52 \times 10^{-3}$ Sv) and suggests that on average, this amount of high salinity waters was mixed in or/and entrained from the lower layer to the upper layer in the strait over the considered time period. Note that current observations in the southern Dardanelles show that the exchange flow there was asymmetrical i.e., the flow was sheared not only vertically but also horizontally. Additionally, it often had a three-layer flow structure (Figure 2c) with brackish upper and salty bottom layers moving toward the Aegean Sea and a salty middle layer flowing toward the Sea of Marmara. This three-layer exchange persisted from a day to a week [*Jarosz et al.*, 2012]. The EPOS observations resolved well the currents vertically at the mooring locations; however, they did not do as well in resolving the horizontal variability of currents in the southern section. Hence, all estimated fluxes of the high salinity waters in the southern part of the strait may have an additional error due to lack of horizontal resolution that might be needed to resolve better the horizontal

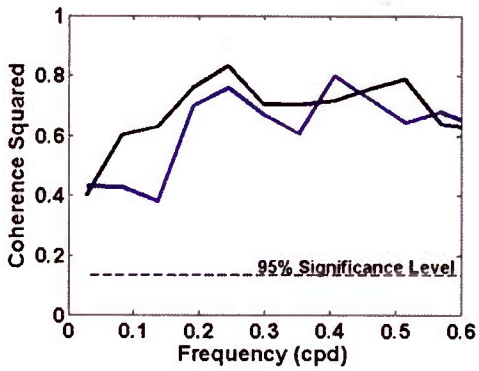

Figure 6. Coherence squared between the fluxes of the lower layer in the northern (blue line) and southern (black line) Dardanelles Strait and the bottom pressure anomaly gradient.

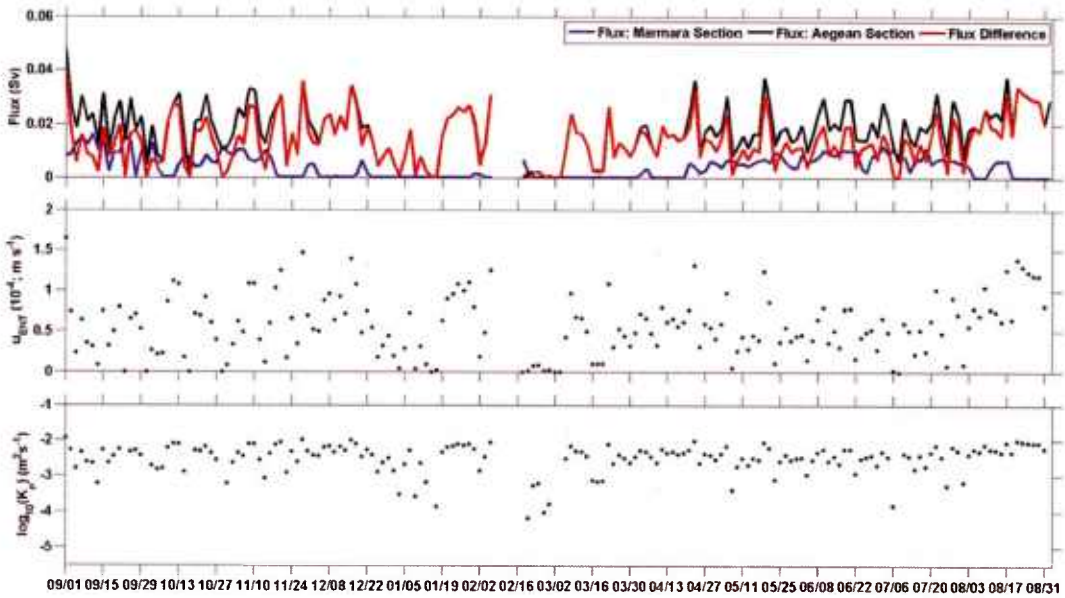

Figure 7. (a) Volume fluxes (Sv) of waters with salinity 39 psu and higher (blue line—Marmara section, black line—Aegean section, and red line—flux difference between the sections); (b) entrainment velocity (m s^{-1}); (c) eddy diffusivity (K_ρ, m^2 s^{-1}).

structure of the outflow of 39-psu waters in the third layer back to the Aegean Sea.

[21] The time series of the volume flux differences of high salinity waters (Q; 48 h averages) was next used to estimate a strait-averaged entrainment velocity and eddy diffusivity (Figures 7b and 7c). For these computations, it was assumed that the average width and length of the Dardanelles Strait are 4 km and 61 km, respectively. The entrainment velocity shown in Figure 7b was found from the following: $u_{ent} = \frac{Q}{Area}$ and, on average, it was 0.55×10^{-4} m s^{-1} and ranged from 0 m s^{-1} to 1.65×10^{-4} m s^{-1}. Following *Kullenberg* [1977], the vertical flux can be expressed as: $u_{ent}\Delta\rho = K_\rho \frac{d\rho}{dz}$, where K_ρ is the eddy diffusivity, ρ is the density, and $\Delta\rho$ is the density difference between the upper and lower layers. This expression led to the eddy diffusivities shown in Figure 7c. The layer-averaged densities, i.e., 1020 kg m^{-3} and 1029 kg m^{-3} for the upper and lower layers, respectively, estimated from our measurements and published historical observations [*Ünlüata et al.*, 1990; *Tuğrul et al.*, 2002] were used in these computations. Strait-averaged K_ρ generally varied from 10^{-4} m^2 s^{-1} to 10^{-2} m^2 s^{-1} with an annual average of 4×10^{-3} m^2 s^{-1}. It is clear from the time series of the eddy diffusivity that there was some variability around the annual mean on short time scales; however, on longer (monthly or seasonal) time scales this variability was much weaker, and, for example, seasonal averages were 4.1×10^{-3}, 3.6×10^{-3}, 3.6×10^{-3}, and 4.5×10^{-3} m^2 s^{-1} for fall 2008, winter 2008/2009, spring 2009, and summer 2009, respectively. Note, K_ρ estimates discussed here are sensitive to a choice of the strait width and densities of the layers.

7. Snapshots of Spatial Variability of Mixing

[22] In February 2009, we twice traversed the Dardanelles Strait from the Aegean exit to the Marmara exit collecting microstructure data under different meteorological and flow conditions. Winds, temperature, salinity, and along-strait velocity components (from the shipboard ADCP) are shown in Figures 8 and 10, while squared buoyancy frequencies (N^2), Richardson numbers (Ri), turbulent kinetic energy (TKE) dissipation rates (ε), and eddy diffusivities (K_ρ) are displayed in Figures 9 and 11.

7.1. February 8 Survey

[23] The February 8 pass through the strait took about 15 h mainly due to ship traffic and challenging weather conditions. Winds were consistently from the southern quadrant for the previous 4 days. The pass began with strong southwesterlies with speeds over 16 m s^{-1} that progressively weakened to about 6 m s^{-1} (Figure 8a) as the Marmara exit was reached. As indicated by currents recorded at M1 and M2, the upper-layer flow in the Aegean section was reversed on 4 February 2009, and then either was extremely weak or blocked before being stopped, and reversed again on 8 February 2009 as shown by along-strait currents recorded by a shipboard ADCP (Figure 8d). The uppermost depth for current observations from the shipboard ADCP was 8 m and, depending on the location along the strait, the deepest depth level was about 80 m, while vertical resolution of these ADCP data was 4 m; thus, these observations did not include any information about near surface and near bottom flows. The reversal of the upper-layer flow persisted beyond the Nara Pass and almost reached the Marmara exit where a near-surface flow (at and above 10 m) in this layer was very weak and mostly directed toward the Sea of Marmara. In winter, the upper-layer waters are characterized not only by low salinity but also by low temperatures as shown in Figure 8b. During the February 8 survey, the low salinity (<30 psu) and temperature

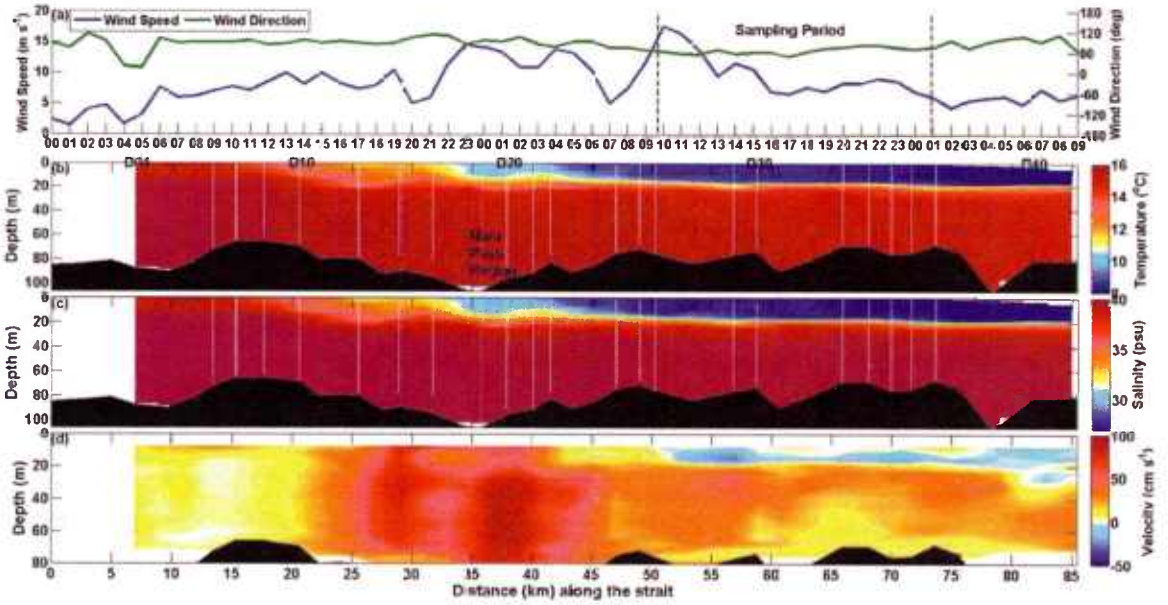

Figure 8. Observations for the February 8 survey: (a) wind speed (m s^{-1}; blue line) and direction (degrees counterclockwise from east) from Çanakkale on 7–9 February 2009 (the horizontal axis indicates GMT hours beginning on 7 February 2009), (b) temperature (°C), (c) salinity (psu), and (d) along-strait current velocities (cm s^{-1}); VMP drops (D04–D41) are marked by white lines in Figures 8b and 8c as well as five drops are identified by their numbers in (b); the VMP sampling period is indicated in (a) and corresponds to plots shown in Figures 8b–8d; the distance along the strait in Figures 8b–8d starts at D01 (near the Aegean exit) and ends at D41 (near the Marmara exit); the bottom in Figures 8b–8d is shown in black.

(<11°C) waters were found in the upper layer between the Nara Pass and the Marmara exit. Farther south, salinity began to increase rapidly. Near the Aegean exit, average salinity and temperature in the upper 10 m of the water column, which is usually occupied by the low salinity outflow, were 38.16 psu and 14.55°C, primarily due to an

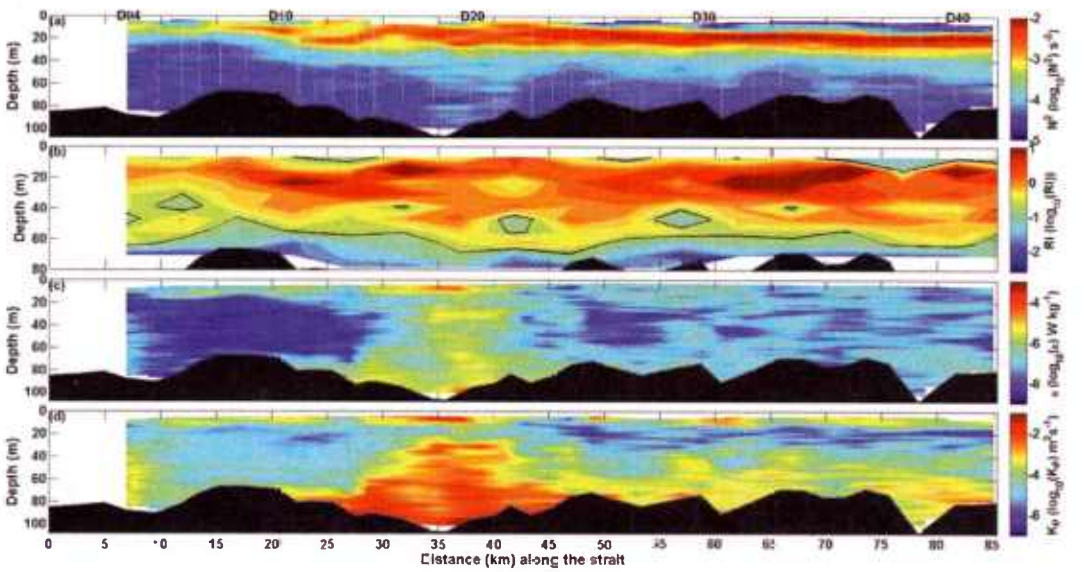

Figure 9. (a) Squared buoyancy frequency (N^2; s^{-2}), (b) Richardson number (Ri), (c) TKE dissipation rate (ε; W kg^{-1}), and (d) eddy diffusivity (K_ρ; m^2 s^{-1}) for the February 8 pass; VMP drops (D04–D41) are marked by white lines and five drops are identified by their numbers in Figure 9a; $Ri = 0.25$ is indicated by a black line in Figure 9b.

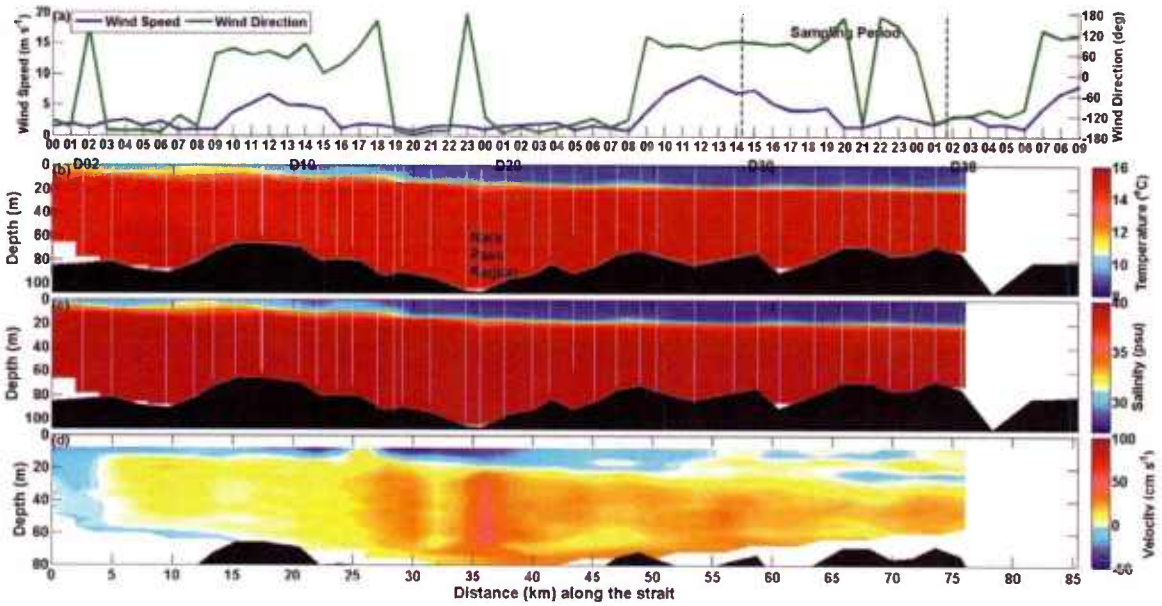

Figure 10. Observations for the February 18 pass: (a) wind speed (m s^{-1}; blue line) and direction (degrees counterclockwise from east) from Çanakkale on 17–19 February 2009 (the horizontal axis indicates GMT hours beginning on 17 February 2009), (b) temperature (°C), (c) salinity (psu), and (d) along-strait current velocities (cm s^{-1}); VMP drops (D01–D38) are marked by white lines in Figures 10b and 10c as well as five drops are identified by their numbers in Figure 10b; the VMP sampling period is indicated in Figure 10a and corresponds to plots shown in Figures 10b–10d; the distance along the strait in Figures 10b–10d starts at D01 (near the Aegean exit) and ends at D41 (near the Marmara exit); the bottom in Figures 10b–10d is shown in black.

influx of warm and salty Aegean waters and mixing associated with the strong winds. Means of the lower-layer salinity and temperature were approximately 39.18 psu and 15.23°C near the Aegean exit, and they were progressively reduced so that near the Marmara exit, these means were 38.76 psu and 14.67°C, respectively.

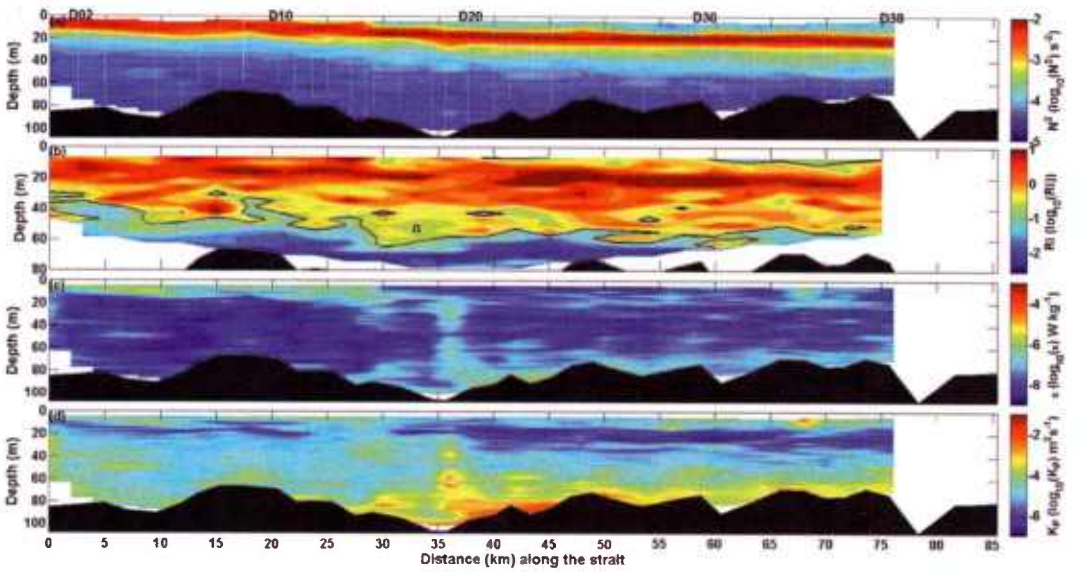

Figure 11. (a) Squared buoyancy frequency (N^2; s^{-2}), (b) Richardson number (Ri), (c) TKE dissipation rate (ε; W kg^{-1}), and (d) eddy diffusivity (K_ρ; m^2 s^{-1}) for the February 18 pass; VMP drops (D01–D38) are marked by white lines and five drops are identified by their numbers in Figure 11a; $Ri = 0.25$ is indicated by a black line in Figure 11b.

[24] The Richardson number ($R_i = N^2\left(\frac{dU}{dz}\right)^{-2}$, where the squared buoyancy frequency is given by: $N^2 = -\left(\frac{g}{\rho}\right)\frac{d\rho}{dz}$, g is the gravitational acceleration, $\frac{dU}{dz}$ is the current shear, and U is the current velocity) is shown for the February 8 survey in Figure 9b. The distribution of this number indicates that mixing generally below 60 m resulted at least partly from shear instabilities ($Ri \leq 0.25$; $\log_{10}(0.25) = -0.6021$ are indicated by black lines in Figures 9b and 11b). Richardson numbers of 0.25 or less were also found in the upper layer. Current velocities from the ship ADCP and $N^2 \geq 10^{-5}$ s^{-2} were used to determine this number for both February 8 and 18 passes. As pointed out before the shipboard current observations did not resolve very well the flows in the upper and lower layers; thus, better measurements are needed to fully determine the variability of the Richardson number in the Dardanelles Strait. The TKE dissipation rates (ε) varied considerably along the strait and were between 10^{-9} W kg^{-1}and 4.8×10^{-4} W kg^{-1} (Figure 9c). Enhanced turbulence was found in the Nara Pass region where all estimated dissipation rates were above 10^{-7} W kg^{-1}with maximum values in the Nara Pass ($\varepsilon > 10^{-4}$ W kg^{-1}above 10 m). In the southern part of the strait, elevated turbulence was observed near the surface and bottom where ε was as high as 10^{-5} W kg^{-1}; however, in the middle of the water column, it was very subdued with the TKE dissipation rates below 10^{-8} W kg^{-1}. The exchange flow north of the Nara Pass toward the Sea of Marmara was more turbulent than that in the southern part of the strait with dissipation rates generally between 10^{-8} W kg^{-1}and 10^{-6} W kg^{-1}.

[25] Following *Osborn* [1980], the eddy diffusivity was estimated from $K_\rho = \gamma\varepsilon N^{-2}$, where γ is a constant related to the mixing efficiency. It has been suggested that γ may not be completely constant particularly when stratification is weak [*Shih et al.*, 2005; *Ivey et al.*, 2008]. For eddy diffusivity estimates discussed here, $\gamma = 0.2$ was used as presented in the vast majority of oceanographic mixing literature [see, e.g., *Osborn*, 1980; *Oakey*, 1982; *Moun*, 1996; *Nash and Moum*, 2001]. *Gregg et al.* [2012] also provide an extensive discussion and justification for this choice of γ. Estimates of K_ρ (Figure 9d) varied broadly in the strait indicating very vigorous mixing ($K_\rho > 10^{-3}$ m^2 s^{-1}) as well as very subdued mixing ($K_\rho < 10^{-5}$ m^2 s^{-1}). Very low values of K_ρ ($< 10^{-5}$ m^2 s^{-1}) were found predominantly between depths of 10 m and 35 m, and they often coincided with depths where the water column was highly stratified (large N, Figure 9a). In the southern part of the Dardanelles Strait, intense mixing was observed above 10 m and near the bottom (below 70 m) where K_ρ was generally from 10^{-4} m^2 s^{-1} to 10^{-3} m^2 s^{-1}, while it was mainly between 10^{-5} m^2 s^{-1} and 10^{-4} m^2 s^{-1} at depths from 30 m and 70 m. The most energetic mixing, which encompassed almost the entire water column, was in the Nara Pass region (mean and median of K_ρ were 1.3×10^{-2} m^2 s^{-1} and 2.7×10^{-3} m^2 s^{-1}, respectively). Here, K_ρ shallower than 10 m and in the bottom boundary layer reached the highest values ($> 10^{-1}$ m^2 s^{-1}). Except for depths between 10 m and 25 m ($N > 0.032$) where the eddy diffusivity dropped below 10^{-4} m^2 s^{-1}, K_ρ was generally above 10^{-3} m^2 s^{-1}. Farther north, mixing was less intense; however, a trend in the vertical K_ρ distribution was preserved, i.e., higher values (10^{-4} m^2 s^{-1} – 10^{-2} m^2 s^{-1}) above 10 m and in the bottom boundary layer and very low eddy diffusivities ($< 10^{-4}$ m^2 s^{-1}) between 10 m and 35 m.

7.2. February 18 Survey

[26] During the February 18 pass, which took about 11.5 h, winds were much lighter than during the February 8 survey. Southerly winds peaked at about 10 m s^{-1} at 12:00 GMT, i.e., 2 h before the survey began (Figure 10a). After that, the southerlies began to subside and then around 20:00 GMT they rotated to westerly and southwesterly with speeds varying between 1.5 m s^{-1} and 3 m s^{-1}. Currents recorded by the shipboard ADCP (Figure 10d) displayed a very complex structure near the Aegean exit, especially in the lower layer where flow was temporarily blocked. There are indications that the currents below 60 m were moving slowly toward the Aegean Sea. Such a complex lower-layer flow structure was also confirmed by current measurements from moorings M1 (Figure 2c) and M2 (data not shown) and was often observed near the southern exit during the deployment period [*Jarosz et al.*, 2012]. Farther inside the strait, the lower-layer flow was well defined and moving toward the Sea of Marmara with maximum along-strait velocities of about 51 cm s^{-1} found in the Nara Pass region. At the same time, the flow in the upper layer was fairly variable and vertically sheared from the Marmara exit to about 10 km north of the Nara Pass. A similar highly sheared upper-layer flow was also recorded by moorings M3 (Figure 2d) and M4 (data not shown). Farther south, the upper-layer flow strengthened to 48 cm s^{-1} near the Nara Pass and the outflow of the low salinity waters was traced throughout the remaining part of the strait through the temperature and salinity observations (Figures 10b and 10c). Minimum salinity and temperature in the upper layer near the northern exit were about 27.95 psu and 8.8°C, respectively, and they progressively increased southward to about 30 psu and 10°C ($S_{mean} = 31.29$ psu and $T_{mean} = 10.85$°C) near the Aegean exit. Lower-layer salinity was as high as 39.19 psu ($S_{mean} = 39.05$ psu), while temperature of these high salinity waters was below 15°C ($T_{mean} = 14.81$°C) near the same exit. Near the Sea of Marmara, the maximum salinity was slightly reduced to 39.07 psu ($S_{mean} = 38.95$ psu), whereas the lower layer was warmer with a maximum temperature of 15.05°C ($T_{mean} = 15.04$°C).

[27] The Richardson number for the February 18 survey is shown in Figure 11b. The distribution of this number indicates that mixing generally below 50 m south of the Nara Pass region and below 60 m in the remaining part of the strait resulted partly from shear instabilities ($Ri < 0.25$) as during the February 8 survey. A Richardson number below 0.25 was also found in the upper layer but only north of the Nara Pass. Unlike during the February 8 survey, turbulence was not highly elevated. These subdued turbulent conditions were reflected in lower values of the estimated TKE dissipation rates that varied between 10^{-9} W kg^{-1}and 7×10^{-6} W kg^{-1} (Figure 11c). In the southern part of the strait, higher ε (4×10^{-7} W kg^{-1}– 7×10^{-6} W kg^{-1}) was found above 10 m. Deeper in the water column, ε began decreasing fairly quickly and below 20 m was primarily between 10^{-9} W kg^{-1} and 10^{-7} W kg^{-1}. Elevated turbulence over almost the entire water column was again found

in the Nara Pass region where all estimated dissipation rates were generally from 10^{-8} W kg^{-1} to 10^{-6} W kg^{-1}with higher values below 15 m ($\varepsilon > 10^{-7}$ W kg^{-1}). North of the Nara Pass, dissipation rates varied between 10^{-9} W kg^{-1}and 10^{-6} W kg^{-1}.

[28] Estimates of K_ρ are shown in Figure 11d. They were generally from 10^{-7} m^2 s^{-1} to 5×10^{-3} m^2 s^{-1}. In the southern part of the Dardanelles Strait, elevated mixing was mostly observed near the surface and near the bottom where K_ρ ranged from 10^{-4} m^2 s^{-1} to 10^{-3} m^2 s^{-1}. In the remaining part of the water column, rather low values of eddy diffusivity ($K_\rho < 10^{-4}$ m^2 s^{-1}) were found. The most energetic mixing, especially below 20 m below the surface, was in the Nara Pass region (mean and median of K_ρ of 10^{-3} m^2 s^{-1} and 4.2×10^{-4} m^2 s^{-1}, respectively). Above 20 m, K_ρ spanned from 7.4×10^{-7} m^2 s^{-1} to 3.1×10^{-5} m^2 s^{-1} (mean and median of K_ρ of 8.1×10^{-6} m^2 s^{-1} and 3.9×10^{-6} m^2 s^{-1}, respectively). Farther north toward the Sea of Marmara, mixing was fairly intense below 60 m with K_ρ varying between 10^{-4} m^2 s^{-1} and 7.4×10^{-3} m^2 s^{-1}. High values of K_ρ were also found above 10 m. In general, the trend in the vertical K_ρ distribution of the February 18 pass was similar to that of the February 8 survey, i.e., higher values above 10 m and in the bottom boundary layer, and depending on location, very low eddy diffusivities ($< 2.6 \times 10^{-6}$ m^2 s^{-1}) at depths where stratification was very stable and strong (Figure 11a).

7.3. Hydraulic Control during February Surveys

[29] Vigorous mixing is commonly observed in ocean straits when compared to mixing on the continental shelves (away from rough topographic features) where vertical eddy diffusivities are typically 10^{-5} m^2 s^{-1} or less [*Ledwell et al.*, 2004; *Oakey and Greenan*, 2004]. For instance, *Wesson and Gregg* [1994] reported K_ρ as high as 10^{-1} m^2 s^{-1} in the Gibraltar Strait. Intense mixing was also found in the Tacoma Narrows of Puget Sound [*Seim and Gregg*, 1997]. *Itoh et al.* [2010] found vertical eddy diffusivities ranging from 3×10^{-5} m^2 s^{-1} to 2×10^{-3} m^2 s^{-1} in the Urup Strait. In the Luzon Strait, *Tian et al.* [2009] reported K_ρ of 10^{-2} m^2 s^{-1} at 500 m. Topographic features, which are very common in straits, such as sills, constrictions, bends, or a permutation of those elements tend to elevate turbulence levels and mixing in their vicinity. They are also known to be locations where the exchange flow may become critical. In the Dardanelles Strait, the most pronounced topographic feature is a combination of a constriction (Nara Pass) and two sharp bends ($\sim 90^o$).

[30] Observations from February 2009 clearly indicate that turbulence and mixing were elevated almost throughout the entire water column in the Nara Pass region. They also imply that the flow was hydraulically controlled in this complex region, i.e., it was supercritical near the first bend from the Aegean section during the February 8 survey when southwesterly winds were strong and the upper-layer flow was reversed past the Nara Pass. The Froude number (F^2) was estimated for a unidirectional two-layer flow with an assumption of the same current velocity in both layers as: $F^2 = \frac{U^2}{r(1-r)g'H}$, where U is the current velocity, H is the channel depth, g' is the reduced gravity ($g' = g\frac{\rho_2 - \rho_1}{\rho_0}$, g is the gravitational acceleration, ρ_1, ρ_2, and ρ_0 are the upper layer, lower layer, and mean density), h_2 is the lower-layer thickness, and $r = \frac{h_2}{H}$ [*Baines*, 1995]. A 35.5 psu isohaline was used to separate the upper and lower layers. It was chosen instead of a 33.64 psu isohaline, which is more consistent with the approach of the layer separation given in *Beşiktepe et al.* [1994] and discussed in section 3, in order to separate the layers as far south as possible of the Nara Pass region (VMP drop D10 was the first location where salinity of the upper layer was below 35.5 psu; see Figure 1 for its location). Mean densities for the upper and lower layers varied from 1026.63 kg m^{-3} and 1029.30 kg m^{-3}, respectively south of the Nara Pass region to 1022.6 kg m^{-3} and 1029.39 kg m^{-3}, respectively near the Marmara end of the strait. Current velocities were between 11 cm s^{-1} and 72 cm s^{-1} with swift flow confined mainly to the Nara Pass region ($U > 47$ cm s^{-1}). The upper layer thickness increased from 10 m at D10 to 23 m near the Marmara exit, while the lower layer was at least 50 m thick. These averages allowed estimations of Froude numbers suggesting that the flow was subcritical ($F^2 < 1$) away from this complex combination of two bends and one constriction. The Froude number increased over 1 indicating that the flow was supercritical near the first bend from the southern end of the strait. Farther north, i.e., toward the next bend and the constriction, F^2 dropped below 1 suggesting a return of the flow to subcritical before beginning an increasing trend again near the Nara Pass ($F^2 = 0.8$).

[31] Data from the February 18 pass, however, did not suggest that the exchange flow became critical anywhere in the strait. For this exchange flow configuration, the composite Froude number ($G^2 = F_1^2 + F_2^2 = \frac{u_1^2}{g'h_1} + \frac{u_2^2}{g'h_2}$, where $F_i^2 = \frac{u_i^2}{g'h_i}$, u_i, and h_i are the internal Froude number, the current velocity, and the thickness for each layer $i = 1, 2$, respectively) was evaluated [*Farmer and Armi*, 1986], and it was less than 1 at all VMP drop locations. The depth of the 33.5 psu isohaline was used to separate layers. Salinity of 33.5 psu was estimated from the approach described in section 3. Mean densities of the upper layer were about 1024 kg m^{-3} and 1022.06 kg m^{-3} near the southern and northern ends of the strait, respectively, while they were 1028.67 kg m^{-3} and 1029 kg m^{-3} for the lower layer near the same locations. u_1 and u_2 were generally below 25 cm s^{-1}, except for the Nara Pass region where currents increased to about 40 cm s^{-1}. The thickness of the upper layer varied from about 9 m near the Aegean end to 21 m near the Marmara end, while the lower layer was generally more than 50 m thick.

[32] Note, that the shipboard ADCP data, which were used in computations of both Froude numbers, were not ideal because the exchange was not well resolved, especially the flow in the upper layer. Additionally, classic internal hydraulic theory was applied to compute Froude numbers. This theory, however, requires a steady state assumption, with no mixing, viscosity, and friction that are not met here since, for instance, mixing could be very vigorous in the Dardanelles Strait.

8. Summary and Conclusions

[33] Current velocity observations collected over 13 months at both ends of the Dardanelles Strait allowed estimations of volume flux time series. These fluxes showed

Table 3. Annual Means of Upper and Lower-Layer Volume Fluxes in 10^{-3}Sv (Positive Values—Flux Toward the Sea of Marmara; Negative Values—Flux Toward the Aegean Sea)

	Northern (Marmara) Section		Southern (Aegean) Section	
Annual Fluxes	Upper Layer	Lower Layer	Upper Layer	Lower Layer
Ünlüata et al. [1990][a,b]	−27.46	17.95	−39.86	30.65
Beşiktepe et al. [1994]	−26.85	17.34	−38.61	29.10
Özsoy and Ünlüata [1997][a,b]	−26.31	16.80	−37.41	27.90
Tuğrul et al. [2002][a,b]	−29.13	18.96	−42.19	32.02
Kanarska and Maderich [2008][c]	−21.14[d]	12.40[d]	−38.82	30.00
EPOS project[a,e]	−25.66	14.02	−36.68	31.67

[a]Fluxes estimated from in situ observations.
[b]Fluxes computed from steady state mass budgets (Knudsen relations).
[c]Fluxes estimated from data obtained from numerical model simulations.
[d]Means approximated from data shown in Figure 6 from *Kanarska and Maderich* [2008].
[e]Fluxes estimated from direct current velocity observations.

distinct temporal variability in both upper and lower layers along both northern and southern sections, especially evident on synoptic time scales. Observed fluctuations were often two or more times larger than estimated annual means. The synoptic flux variability in the upper layer was coherent with the local atmospheric forcing and the bottom-pressure anomaly gradient. In the lower layer, flux variations were related to variations of the bottom-pressure anomaly gradient. Note that the atmospheric forcing and the pressure anomaly gradient were not able to explain all observed variability, which could be partially related to dynamical processes inside the strait and/or in the adjacent seas.

[34] Volume fluxes also varied weakly on longer time scales (monthly to seasonal). Moreover, seasonal means imply that the upper-layer fluxes were at a maximum in spring and at a minimum in fall, while the opposite was true for the lower-layer fluxes. The maximal inflow in the lower layer to the Dardanelles Strait from the Aegean Sea and the minimal outflow in the upper layer during fall differ from the lower and upper-layer fluxes during fall discussed by *Tuğrul et al.* [2002] who calculated volume fluxes from hydrological data using Knudsen's approach expressing the steady state mass budget. Their estimates show that both upper and lower-layer fluxes are at a minimum in fall. The seasonal variability is also different from modeling results presented by *Kanarska and Maderich* [2008]. They report that the upper layer flux is at a maximum in winter and at a minimum in summer, while again the opposite is true for the lower layer fluxes. Annual means (Table 3) evaluated from the flux time series are in a good agreement with those estimated by the other researchers, especially in the southern Dardanelles section. Table 3 lists a few volume fluxes calculated by other research groups for comparison with the fluxes computed from the observations of the EPOS project.

[35] The flux estimates also indicated that there was a net volume flux of low salinity waters from the strait. This flux displayed a great deal of variability in amplitude and direction throughout the deployment time period; however, its annual mean, which is within a 95% confidence interval of those cited in literature [for instance, *Ünlüata et al.*, 1990; *Beşiktepe et al.*, 1994; *Tuğrul et al.*, 2002], clearly showed a net outflow to the Aegean Sea. There was also seasonal variability in the net outflow of low salinity waters that peaked during spring 2009, which is in agreement with findings of *Tuğrul et al.* [2002].

[36] The volume flux of high salinity waters (salinity of 39 psu and higher) was also utilized to evaluate strength of mixing in the Dardanelles Strait. These computations indicate that there was elevated mixing in this strait with strait-averaged eddy diffusivities ranging from 10^{-4} m^2 s^{-1} to 10^{-2} m^2 s^{-1}. During two passes through the Dardanelles in February 2009, microstructure observations were collected under different meteorological and exchange flow conditions and were used to estimate eddy diffusivity. The strait averaged estimates of K_ρ for February 8 and February 18 surveys were 1.9×10^{-3} m^2 s^{-1} (median of 10^{-4} m^2 s^{-1}and standard deviation of 1.4×10^{-2} m^2 s^{-1}) and 1.8×10^{-4} m^2 s^{-1} (median of 1.9×10^{-5} m^2 s^{-1}and standard deviation of 8.3×10^{-4} m^2 s^{-1}), respectively. These values generally agree with the values calculated using the high salinity entrainment velocity approximation over the entire deployment period.

[37] The February surveys clearly showed that mixing in the Dardanelles Strait varied spatially and temporarily, and was dependent on complex strait geometry, exchange flow status, and partially on meteorological conditions. High values of vertical eddy diffusivities as well as vigorous mixing were found in the Nara Pass region. For example, estimates of K_ρ for the February 8 pass were as large as 4.6×10^{-1} m^2 s^{-1} with a depth averaged mean of 1.7×10^{-2} m^2 s^{-1}. Energetic mixing was generally observed above 10 m and near the bottom (usually below 60 m). Vertical distributions of eddy diffusivities were generally almost identical for all VMP drops, i.e., higher values of K_ρ were mainly above 10 m and near the bottom. The lowest eddy diffusivities were frequently at depths where stratification was very stable (large N was usually observed at depths between 10 m and 35 m).

[38] The Froude number is a key parameter of internal hydraulic theory. This theory is one of analytical solutions that are used to predict fluxes of exchange flows in straits. Estimates of Froude numbers from the February observations suggested that the exchange flow in the Dardanelles Strait could be temporarily hydraulically controlled in the Nara Pass region. Another analytical approach referred by *Hogg et al.* [2001] as the viscous-advective-diffusive (VAD)

solution applies in straits where the exchange is dominated by turbulent mixing. For this solution, there are three important parameters: the aspect ratio $A = \frac{H}{L}$, the turbulent Grashof number $Gr_T = \frac{g' H^3}{K_\nu^2}$, and turbulent Prandtl number $Pr_T = \frac{K_\nu}{K_\rho}$, where H (60 km) and L (55m) are the channel depth and length, g' is the reduced gravity ($g' = g\frac{\Delta\rho}{\rho_0}$, where g is the gravitational acceleration, $\Delta\rho$ is the density difference between two ends of the strait, and ρ_0 is the reference density), K_ν and K_ρ are the eddy viscosity and diffusivity, respectively. *Hogg et al.* [2001] proposed the nondimensional parameter, $Gr_T A^2$, to characterize hydrodynamics of exchange flows in straits. Note that the two analytical solutions represent two extreme limits and between them there is a vast range of flows which cannot be represented accurately by either. If $Gr_T A^2 > 10^5$ the hydraulic limit gives a good estimate of the volume flux. The VAD theory provides an approximation of the flux for $Gr_T A^2 < 40$. $Gr_T A^2$ was 4.2×10^3 ($g' = 0.03$ m s^{-2}, strait averaged $K_\nu = 10^{-3}$ m^2 s^{-1}) and 1.1×10^5 ($g' = 0.008$ m s^{-2}, strait averaged $K_\nu = 10^{-4}$ m^2 s^{-1}) for the February 8 and February 18 passes, respectively. The estimate of $Gr_T A^2$ for the February 8 is virtually identical to that computed from the modeling output by *Kanarska and Maderich* [2008] indicating that the exchange flow in the Dardanelles Strait was in the intermediate regime and the volume flux was neither in the hydraulic nor the VAD limit. Observations from 18 February 2009, however, seem to imply that the exchange was close to the two-layer hydraulic regime.

[39] Observations presented in this paper clearly show that variability of the volume flux, mixing, and flow structure in the Dardanelles Strait is very complex and can be highly impacted by variability of hydrographic and atmospheric conditions. Our understanding of short and long-term processes responsible for those variations is still very limited and requires further studies. Hence, more detailed observational and modeling efforts encompassing the entire strait and done, for instance, under a variety of atmospheric and oceanographic conditions are necessary to fully understand processes governing exchange dynamics in this strait.

[40] **Acknowledgments.** This work was supported by the Office of Naval Research as a part of the NRL's basic research project "Exchange Processes in Ocean Straits (EPOS)." We would like to thank everyone from the NATO CMRE (previously known as the NATO NURC) who supported and helped to organize and fund cruises to the TSS on the R/V Alliance. We are also grateful for the outstanding assistance and help received from the personnel of the Turkish Navy Office of Navigation, Hydrography, and Oceanography. We would like to thank Mark Hulbert, Andrew Quaid, Wesley Goode, and Steve Sova, our technicians, for excellent instrument preparation, mooring deployment, and mooring recovery. We are also thankful and indebted to the crew of the R/V Alliance for assisting with our mooring deployment and recovery in very challenging conditions.

References

Baines, P. G. (1995), *Topographic Effects in Stratified Flows*, Cambridge Univ. Press, Cambridge, U. K.

Beşiktepe, Ş. T., E. Özsoy, and Ü. Ünlüata (1993), Filling of the Marmara Sea by the Dardanelles lower layer inflow, *Deep Sea Res., Part I*, *40*, 1815–1838.

Beşiktepe, Ş. T., H. I. Sur, E. Özsoy, M. A. Latif, T. Oğuz, and Ü. Ünlüata (1994), The circulation and hydrography of the Marmara Sea, *Prog. Oceanogr.*, *34*, 285–334.

Beşiktepe, Ş. T. (2003), Density currents in the two-layer flow: An example of Dardanelles outflow, *Oceanol. Acta*, *26*, 243–253.

Farmer, D. M., and L. Armi (1986), Maximal two-layer exchange over a sill and through the combination of a sill and contraction with barotropic flow, *J. Fluid Mech.*, *164*, 53–76.

Gertman I., N. Pinardi, Y. Popov, and A. Hecht (2006), Aegean Sea water masses during early stages of the Eastern Mediterranean Climatic Transient (1988–1990), *J. Phys. Oceanogr.*, *36*, 1841–1859.

Gregg, M. C., M. H. Alford, H. Kontoyiannis, V. Zervakis, and D. Winkel (2012), Mixing over the steep side of the Cycladic Plateau in the Aegean Sea, *J. Mar. Syst.*, *89*, 30–47, doi:10.1016/j.jmarsys.2011.07.009.

Hogg, A. M., G. N. Ivey, and K. B. Winters (2001), Hydraulics and mixing in controlled exchange flows, *J. Geophys. Res.*, *108*, 959–972.

Itoh, S., I. Yasuda, T. Nakatsuka, J. Nishioka, and Y. N. Volkov (2010), Fine- and microstructure observations in the Urup Strait, Kuril Islands, during August 2006, *J. Geophys. Res.*, *115*, C08004, doi:10.1029/2009JC005629.

Ivey, G. N., K. B. Winters, and J. R. Koseff (2008), Density stratification, turbulence, but how much mixing?, *Ann. Rev. Fluid Mech.*, *40*, 169–184.

Jarosz, E., W. J. Teague, J. W. Book, and S. T. Beşiktepe (2012), Observations on the Characteristics of the Exchange Flow in the Dardanelles Strait, *J. Geophys. Res.*, *117*, C11012, doi:10.1029/2012JC008348.

Kanarska, Y., and V. Maderich (2008), Modelling of seasonal exchange flows through the Dardanelles Strait, *Estuarine Coastal Shelf Sci.*, *79*, 449–458, doi:10.1016/j.ecss.2008.04.019.

Kara, A. B., A. J. Wallcraft, H. E. Hulbert, and E. V. Stanev (2008), Air-sea fluxes and river discharges in the Black Sea with a focus on the Danube and Bosphorus, *J. Mar. Syst.*, *74*, 74–95.

Kullenberg, G. (1977), Entrainment velocity in natural stratified vertical shear flow, *Estuarine Coastal Mar. Sci.*, *5*, 329–338.

Ledwell, J. R., T. F. Duda, M. A. Sundermeyer, and H. E. Seim (2004), Mixing in a coastal environment: 1. A view from dye dispersion, *J. Geophys. Res.*, *109*, C10013, doi:10.1029/2003JC002194.

Moun, J. N. (1996), Efficiency of mixing in the main thermocline, *J. Geophys. Res.*, *101*, 12,057–12,069.

Nash, J. D., and J. N. Moun (2001), Internal hydraulic flows on the continental shelf: High drag states over a small bank, *J. Geophys. Res.*, *106*, 4593–4611.

Oakey, N. S. (1982), Determination of the rate of dissipation of turbulent energy from simultaneous temperature and velocity shear microstructure measurements, *J. Phys. Oceanogr.*, *12*, 256–271.

Oakey, N. S., and B. J. W. Greenan (2004), Mixing in a coastal environment: 2. A view from microstructure measurements, *J. Geophys. Res.*, *109*, C10014, doi:10.1029/2003JC002193.

Osborn, T. R. (1980), Estimates of the local rate of vertical diffusion from dissipation measurements, *J. Phys. Oceanogr.*, *10*, 83–89.

Özsoy, E., and Ünlüata, Ü. (1997), Oceanography of the Black Sea: A review of some recent results, *Earth Sci. Rev.*, *42*, 231–272.

Peneva, E., E. Stanev, V. Belokopytov, and P. Y. Le Traon (2001), Water transport in the Bosphorus Strait estimated from hydro-meteorological and altimeter data: Seasonal and decadal variability, *J. Mar. Syst.*, *31*, 21–33.

Poulos, S. E., P. G. Drakopoulos, and M. B. Collins (1997), Seasonal variability in sea surface oceanographic conditions in the Aegean Sea (Eastern Mediterranean): An overview, *J. Mar. Syst.*, *13*, 225–244.

Seim, H. E., and M. C. Gregg (1997), The importance of aspiration and channel curvature in producing strong vertical mixing over a sill, *J. Geophys. Res.*, *102*, 3451–3472, doi:10.1029/96JC03415.

Shih, L. H., J. R. Koseff, G. N. Ivey, and J. H. Ferziger (2005), Parameterization of turbulent fluxes and scales using homogeneous sheared stably stratified turbulence simulations, *J. Fluid Mech.*, *525*, 193–214.

Simonov, A. I., and E. N. Altman (1991), Hydrometeorology and hydrochemistry of the USSR seas, in *Sensitivity to Change: Black Sea, Baltic Sea and North Sea, NATO/ASI Ser.*, vol. IV, edited by E. Özsoy and A. Mikaelyan, pp. 11–25, Kluwer Acad., Dordrecht, Netherlands.

Tian, J., Q. Yang, and W. Zhao (2009), Enhanced diapycnal mixing in the South China Sea, *J. Phys. Oceanogr.*, *39*, 3192–3203.

Tuğrul, S., Ş. T. Beşiktepe, and İ. Salihoğlu (2002), Nutrient exchange fluxes between the Aegean and Black Seas through the Marmara Sea, *Mediter. Mar. Sci.*, *3/1*, 33–42.

Tzali, M., S. Sofianos, A. Mantziafou, N. Skliris (2010), Modelling the impact of Black Sea water inflow on the North Aegean hydrodynamics, *Ocean Dyn.*, *60*, 585–596, doi:10.1007/s10236-010-0277-3.

Ünlüata, Ü., T. Oğuz, M. A. Latif, and E. Özsoy (1990), On the physical oceanography of the Turkish Straits, in *The Physical Oceanography of Sea Straits, NATO/ASI Ser.*, edited by L. J. Pratt, pp. 25–60, Kluwer Acad., Dordrecht, Netherlands.

Wesson, J. C., and M. C. Gregg (1994), Mixing at Camarinal Sill in the Strait of Gibraltar, *J. Geophys. Res.*, *99*, 9847–9878, doi:10.1029/94JC00256.

Wolk, F., H. Yamazaki, L. Seuront, and R. G. Lueck (2002), A new free-fall profiler for measuring biophysical microstructure. *J. Atmos. Oceanic Technol.*, *19*, 780–793.

Zervakis, V., D. Georgopoulos, and P. G. Drakopoulos (2000), The role of the North Aegean in triggering the recent Eastern Mediterranean climatic changes, *J. Geophys. Res.*, *105*, 26,103–26,116.